

Effect of monomer precursors with identical functionality on the properties of the physical network

Ariana Torres-Knoop¹, Verena Schamboeck², Nitish Govindarajan^{2,3},
Pieter D. Iedema², and Ivan Kryven^{4,5*}

¹SURFsara, Science Park 140, 1098 XG Amsterdam, the Netherlands

²Van 't Hoff Institute for Molecular Sciences, University of Amsterdam, the Netherlands

³Department of Physics, Technical University of Denmark, 2800 Kgs Lyngby, Denmark

⁴Mathematical Institute, Utrecht University, Budapestlaan 6, 3508 TA Utrecht, the Netherlands

⁵Centre for Complex Systems Studies, 3584 CE Utrecht, the Netherlands

August 3, 2022

Abstract

Thermo-mechanical properties of polymer networks are known to depend on the functionality of monomer precursors – an association that is frequently exploited in materials science. We use molecular simulations to generate physical networks from chemically different monomers with identical functionality and show that such networks have several universal graph-theoretical properties as well as near universal Young's modulus, whereas the vitrification temperature is universal only up to a certain density of the network, as measured by the bond conversion. The latter observation is explained by noticing that monomer's tendency to coil is shown to enhance formation of topological holes, which, when accumulated in the network, result in a phase transition marked by the emergence of a percolating cell complex restricting network's mobility. This higher-order percolation occurs late after gelation and is shown to coincide with the onset of brittleness indicated by a sudden increase in the glass transition temperature.

Keywords Network, Cycles, Cell Complex, Molecular Simulations

1 Introduction

The structure of polymer networks defines physical properties of the material,¹ however, the formation of such networks is poorly understood. This process is driven by the reaction kinetics and physical chemistry, and, at the same time, the kinetics itself is mediated by the evolution of the polymer network and its emergent geometry. Molecular dynamics (MD) simulations can be used to generate the geometry and topology of networks and their effect on the thermo-mechanical properties. Jung *et al.*² used MD simulations to study the chain-growth polymerisation of the monofunctional methyl methacrylate (MMA) and reported volume shrinkage and glass transition temperatures. Demir *et al.*³ and Huang *et al.*⁴ employed MD to simulate copolymerisation of the vinyl ester/styrene polymer network. They reported structural polymer properties, such as the formation of cycles, the glass transition and Young's modulus. Klähn *et al.*⁵

studied the effect of different monofunctional (meth)acrylate monomers on the glass transition temperature using molecular simulations. Rudyak *et al.*⁶ studied the effect of the initiator concentration on a chain-growth polymer network and reported gel conversions, gel fractions and cycle length distributions. In our previous study, we established a simulation protocol for polymerisation of 1,6-hexanediol diacrylate (HDDA), and observed the formation of 'short cycles' during the polymerisation process: small cycles were created in primary and secondary cyclization reactions and were promoted by enhanced monomer flexibility.⁷ On the one hand, the ability to form cycles is dictated by the local conformational dynamics of monomers, namely by the torsional strain and steric hindrance. On the other hand, these reactions influence the global properties of the network, such as the density and excluded volume by introducing topological defects that are elastically inactive. Therefore, different monomers with identical number of functional groups may lead to differ-

ent gelation times and elastomeric properties of the network. Since monomer structures can be readily manipulated, understanding the mechanism behind the monomer influence on the final polymer network is a fundamental question for enabling rational material design.

The problem of optimising elastic modulus and glass transition temperature arises in different contexts, for example, when designing self-healing materials,⁸ but also in lithography, coatings for biomaterials, textiles and dental composites.^{9–15} Acrylate polymers assemble into linear chains, when monomers carry one vinyl group, or crosslinked networks – several vinyl groups per monomer¹⁶ and can be tuned by adjusting different substituents in the α -carbon, linkers between the vinyl groups, and by adding functional groups.¹⁷

In this work we perform a screening study of a range of di-functional (meth)acrylates, see Figure 1, with different linker length using molecular simulations. These monomers bear two double bonds, which allow them to appear in the final network as nodes with 0, 1, 2, and 4 connections. The only difference lies in the length of the linker between the double bonds and the presence or absence of a bulky non-functional group close to the radical site (methyl substituent). Standard theories that coarse-grain monomers by ignoring their structural formulas hypothesise universal network properties for all of these monomers.^{18–21} Although such coarse-grained theories are irreplaceable when studying the rates of multiple competing reactions, or tuning species concentrations, the purpose of this work is to put this hypothesis under scrutiny and investigate if subtle changes to nonreactive parts of monomers may nevertheless reflect on the structure of the polymer network, and therefore, on the thermo-mechanical properties of the polymer.

In Results, we report physical properties related to diffusion, glass transition and elasticity. Then, we turn to the topological analysis of the network and its emergent geometry and match the structural changes in the network with the development of the physical properties. We show universality across different monomer types with respect to such properties as the degree distribution, cyclomatic number, gel point conversion, and Young’s modulus. We also report that such universality is broken in dense networks, as can be seen by diverging glass transition temperatures associated to different monomer types. We show that this divergence may be mediated by small chordless cycles, also called topological holes, and report two qualitative transitions in the network structure. The first transition – gelation, is marked by appearance of an extensive cluster and is responsible for emergence of elastic behaviour. The second transition, is marked by emergence of an extensive higher-order topological entity called a *cell complex*, and is associated with a steep increase of glass transition temperature that may cause an onset of brittleness.

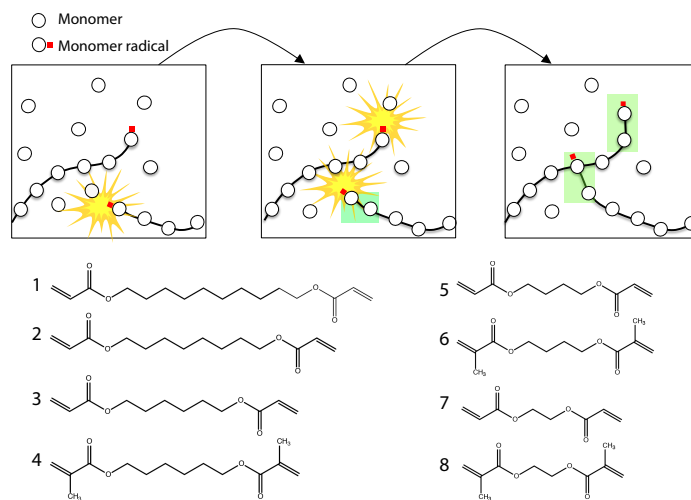


Figure 1: **Radical polymerisation of diacrylate monomers.** The network grows only at a few locations called *monomer radicals* (labelled with ■). When reacting, a monomer radical and another node become connected. A node may obtain maximum 4 connections as it is identified with one of the following acrylate monomers: 1) 1,10-decanediol diacrylate (DDDA), 2) 1,8-octanediol diacrylate (ODDA), 3) 1,6-hexanediol diacrylate (HDDA), 4) 1,6-hexanediol dimethylacrylate (HDDMA), 5) 1,4-butyldiol diacrylate (BDDA), 6) 1,4-butyldiol dimethylacrylate (BDDMA), 7) 1,2-ethylenediol diacrylate (EDDA), 8) 1,2-ethylenediol dimethylacrylate (EDDMA).

Results

Polymerisation process

During radical polymerisation, initially disconnected monomer units join together to form a growing network through three main reactions: initiation, propagation, and termination. As a matter of convention, we visualise these processes by representing monomers as labelled nodes of various functionality that receive connections according to special rules, as shown in Figure 1. However, the real radical polymerisation is a process that is also affected by the microscopic properties, *e.g.*, monomer mobility and geometry, as well as by the macroscopic topological and thermo-mechanical changes in the whole system, *e.g.*, viscosity, gelation, glass transition, volume shrinkage and overall density. We study this process with dynamical systems that govern the motion of all atoms individually. Methods section explains the set-up of our curing simulations and the validation of the force field model.

Diffusion

In growing polymer networks, reactions rapidly become diffusion limited. Let us define bond conversion $0 \leq \chi(t) \leq 1$ as the ratio between the formed covalent bonds at time t and the maximal number of covalent bonds that the system may contain. Since each monomer can have maximum 4 neighbours, and each radical reduces the total number of bonds by 2, we have:

$$\chi(t) = \frac{b(t)}{2N_{\text{sys}} - R_0},$$

where $b(t)$ is the current number of bonds, $R_0 = 100$ the initial number of radicals, and $N_{\text{sys}} = 2000$ the number of monomers in the system. Figure 2a quantifies the kinetic slowdown $\chi(t)$ for each monomer type, where we observe that: (1) for a given linker length, the presence of a methyl substituent significantly slows down bond formation, (2) for a given substituent, the polymerisation process slows down with increasing linker length, and (3) the mobility of all systems slows down with curing. In Supplementary Figure S4, we also present a comparison of the monomer diffusion coefficients as a function of conversion for systems with and without a methyl substituent. These results show that the decrease in the speed of polymerisation is affected by the overall reduced translational mobility of bulkier dimethacrylates. One can also conclude from the radial distribution functions (RDFs) in the melt state, shown in Supplementary Figure S5, that the addition of a methyl substituent reduces the frequency of reactions, as reactions involving the α -carbon become less likely due to the steric effects. The analysis of the RDFs suggests that shielding a radical site by longer linkers is negligible, see Supplementary Figure S6, which was also pointed out by Kurdikar and Peppas.²² Therefore the diffusion of free monomers might play a dominant contribution to

the overall kinetic slowdown, see Supplementary Figure S7, which constitutes perhaps the strongest difference between the studied monomer types.

After confirming that chemical reactions take place on different time scales for different monomers, in what follows we report all results as a function of bond conversion χ instead of time. In this way we focus on the outcome of the polymerisation and not merely on its absolute speed.

Thermomechanics

T_g is determined by analysing the inverse density as a function of temperature.²³ As illustrated in Figure 2b and explained in Methods, we search for such a temperature, where this function fails to be smooth. As shown in Figure 2c, T_g increases with bond conversion for all monomers. The increase is first linear and well-explained by a *universal* relationship across all monomer species:

$$T_g(\chi) = A\chi + T_{g,0}, \quad A = 155\text{K},$$

when $\chi < 0.7$. The linear trend is abruptly broken at higher bond conversions. In the Topology section, we argue that a novel higher-order percolation transition provides an explanation for such an abrupt change of T_g . The data presented in Figure 2c suggest that shorter linkers might promote higher T_g for $\chi > 0.7$.

Both observations, the linear dependence and the deviation that follows it, are in line with findings in literature. Bowman *et al.*²⁴ reported the T_g for the homo- and copolymerisation of DEGDA and DEGDMA with monofunctional monomers (n-octyl methacrylate and n-heptyl acrylate, respectively). These authors observed an increase in T_g with increasing crosslinker density. Jerolimov *et al.*²⁵ studied the effect of divinyl crosslinking agents with different chain length (EGDMA and TEGDMA) on the T_g of PMMA and also reported a similar observation.

Elasticity

Young’s modulus, can be determined by estimating the slope of the stress-strain curve in the linear region, when a sample is pulled at a constant rate in the static tensile test. Since the test is performed under conditions of thermal fluctuations, see Figure 2d, statistical methods are used to infer the linear region and its slope, see the Methods section.

Figure 2e shows that for all monomer systems Young’s moduli increase linearly as a function of bond conversion:

$$E(\chi) = B(\chi - \chi_0),$$

featuring a universal slope $B = 3.6\text{GPa}$, with χ_0 being the largest χ , for which $E = 0$. Parameter χ_0 turns out to be weakly dependant on linker length: Monomers with longer linker length feature smaller values of the moduli with an exception of HDDA-BDDA pair that deviates from the universal behaviour for $\chi < 0.6$ showing a reverse order. The overall

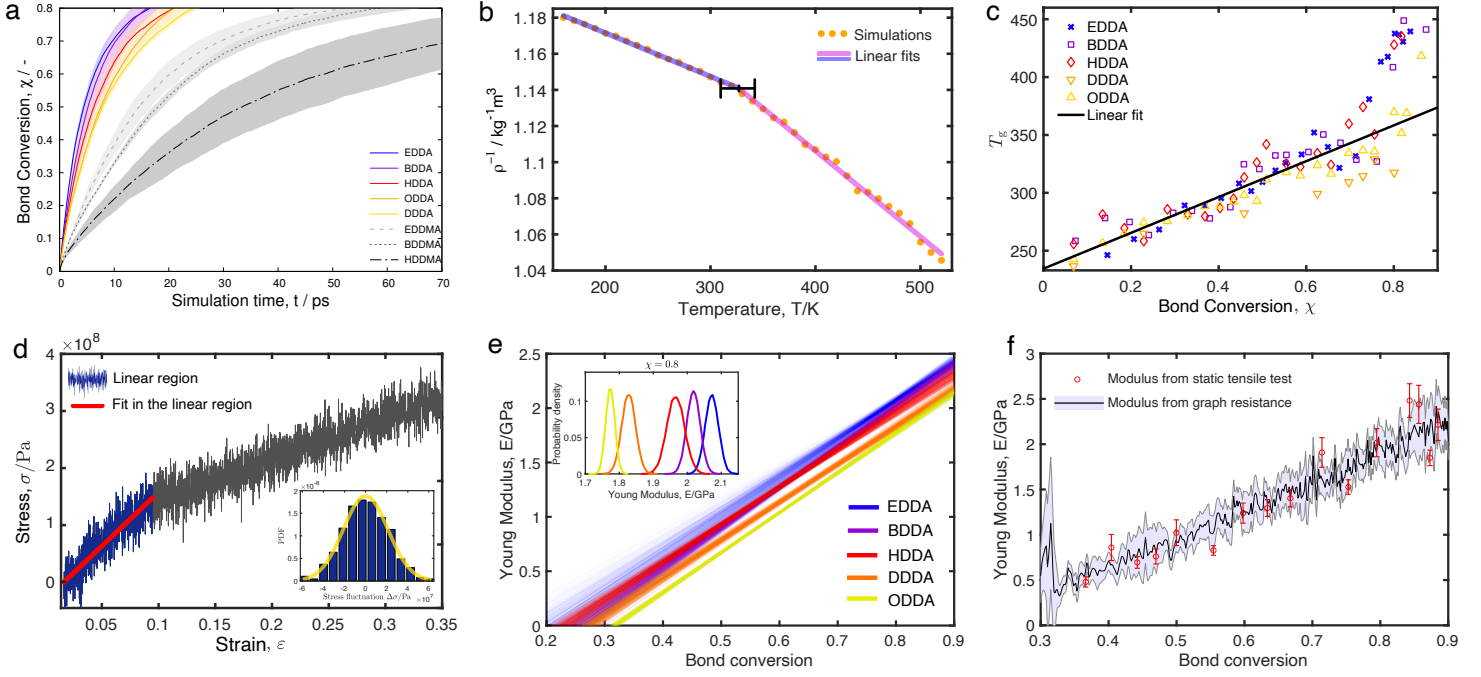


Figure 2: **Inferring species diffusion and thermo-mechanical properties from molecular simulations** (a) Bond conversion as a function of simulation time for different monomers. Confidence intervals indicate one standard deviation. (b) Procedure for calculating T_g as the break point for a piece-linear fit of the inverse density, ρ^{-1} , see Methods for details. (c) When plotted versus bond conversion, T_g features a universal collapse to a linear dependence $T_g(\chi) = A\chi + T_{g,0}$, where $\chi < 0.8$ for monomers without methyl group. The solid line indicates a linear fit with an estimated slope $A = 155\text{K}$. Supplementary Figure S14 reports confidence intervals for these data. (d) The stress-strain curve with a thermal noise is processed to identify the region of initial linear growth and its slope, see Methods for details. The deviations from the fit, shown in the inset, are confirmed to be normally distributed and not autocorrelated. (e) Young's modulus feature a linear dependence on bond conversion resulting in fuzzy linear fits due to thermal fluctuations. The cross-sections of the probability densities of the fits at final bond conversion $\chi = 0.8$ are shown in the inset. Supplementary Figure S15 reports confidence intervals. (f) Prediction of Young's modulus from solely spectral graph properties of the network, is shown for the HDDA monomer. See Supplementary Figure S17 for resistance-elastic moduli comparison for other monomers. The elastic modulus and T_g were averaged over four simulation runs.

effects of the crosslinker length and bond conversion on elasticity are in agreement with experimental findings.^{26,27}

The evolution of the elastic modulus is universally explained for all monomers by a spectral property of the networks called *graph resistance*, see Methods for calculations. Figure 2f compares the modulus obtained from the tensile test and the scaled graph resistance for on an example of HDDA. As shown in Supplementary Figure S17, presenting this comparison for other monomers, the graph resistance has to be scaled by a constant that absorbs the contribution from single monomer tendency to coil and ranges between 5.0 and 8.8GPa.

Topology

As a result of polymerisation, monomers join together with covalent bonds forming dense polymer networks, for example, as the series shown in Figures 3a for DDDA system. So far, we have discussed emergent physical properties of the polymer related to diffusion, density, and elasticity. For all of these quantities apart of the monomer diffusion coefficient, the number of bonds was a more important determining factor than the chemical type of the monomer. Such an observation points out a hypothesis that the physical properties under investigation are predominantly defined by the network structure, and only indirectly, by the monomer type. In other words: the network acts as an intermediate link between the monomer chemistry and the macroscopic physics.

We quantify the structure of polymer networks in terms of several notions common to topology and (spectral) graph theory. Namely, we look at degree distribution, graph resistance, connected components, cycles, holes, and cell complexes. We analyse the dependence of these quantities on the monomer type, and argue about their effect on the emergent physical properties.

Our first finding is that *self loops* form frequently, as caused by a radical reacting with the pending vinyl group of the same monomer. Each self-loop decreases the maximum degree of one monomer from 4 to 2, and therefore self loops are of general interest in reaction kinetics and material science, where they are often referred to as topological defects.^{28–32} In a similar fashion, a *double edge* occurs when a pair of monomers reacts twice, thus becoming connected with two bonds, which limits their external number of neighbours to 4 per pair, instead of 6. As Figure 4a suggests, a shorter linker between the functional groups promotes formation of self loops and a very similar trend is observed for double edges, see Figure 4b. This observation holds with one exception of HDDA. An initio and classical simulations presented in Supplementary Figure S3 and Supplementary Figure S13 suggest that the exception might be related to a coiled metastable state of HDDA – the end-to-end distance being close to the reaction cutoff radius. Moreover, the ability to form triangles – cycles of size three – is also enhanced by short linkers, see Supple-

mentary Figure S10, again with the BDDA-HDDA pair being swapped in the order of the trend.

As shown in Supplementary Figure S9 the effect of the methyl substituent is less clear: For EDDMA, the methyl substitution induces more loops, but for the other two linker lengths (BDDMA and HDDMA) the results are inconclusive. The end-to-end distance probability distribution of the pure monomers, shown in Supplementary Figure S2, suggests that the larger number of self loops in EDDMA could also be caused by a metastable coiled configuration of this molecule.

Such a strong influence of monomer types on forming cyclic structures is characteristic only to the smallest scale. To demonstrate this, we compute the maximum number of edges one can remove before the network becomes composed of tree components – the cyclomatic complexity r , which can be calculated from the relationship $r = M - N + C$ with M being the total number of edges, N – number of nodes, and C – number of connected components in the network. Clearly, self loops, double edges, and triangles increase cyclomatic complexity. As shown in Figure 4c, all monomers lead to a comparable cyclomatic complexity, where about 10% of this quantity is explained by the self-loops and double edges alone. In order to investigate higher order cyclic structures, we must differentiate between a *cycle*, which is a closed path in a graph, and a *hole* – a cycle for which any subpath is also the shortest path connecting the endpoints.

Bonds that are not self loops, connect different nodes together and thus extend network in its size. By computing the degree distribution, that is fractions of nodes having different number of neighbours, we again observe a universal behaviour across monomer types, shown in Figure 4e. The dynamics seen in Figure 4e is different from the binomial degree distribution, which is characteristic to standard bond percolation,^{18,20,21,33} but dictated by the chain growth polymerisation.³⁴ The degrees of monomers with methyl substituents are analysed in Supplementary Figure S8, showing that the presence/absence of the methyl group does not have a significant effect on the degree distribution. This is in strong contrast to the observed differences in polymerisation properties for different monomer types when studied as a function of time, for example as in Figure 2a, where such differences are mainly attributed to diffusion limited nature of the reaction. Figure 4e gives reason to suggest that the diffusion effects do not strongly influence the density of the network when viewed as a function of *bond conversion*.

Self loops and small cycles are in competition with forming bonds that expand the network size. Although formation of small cycles do not significantly affects the degree distribution, they delay the onset of *gelation*, that is the moment in time when an extensive connected component emerges. Note that the mean-field theories predict the gel point exclusively on the basis of the degree distribution,^{18,20,21,35,36} which unlike self loops and small cycles, was shown to be insensitive to the monomer type. The onset of gelation is

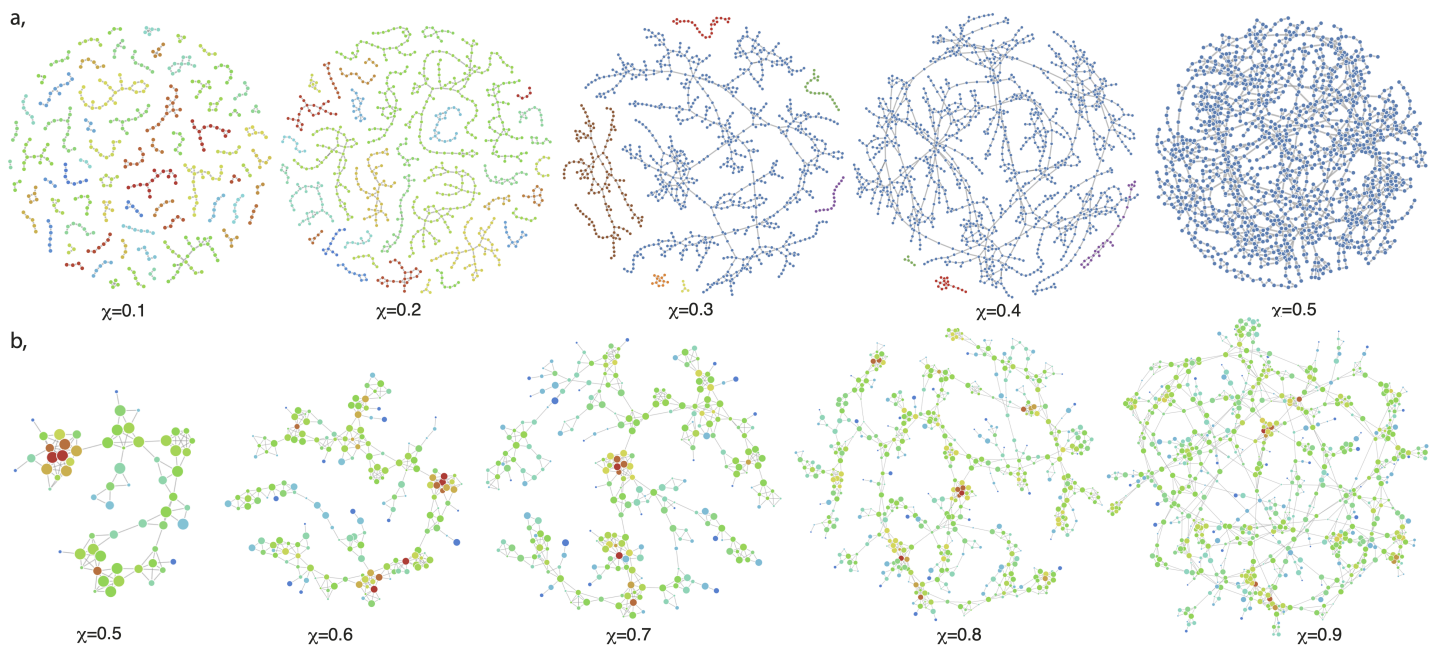


Figure 3: **Two-dimensional representation of the network and cell-complex developing during free-radical polymerisation of DDDA.** (a) Network structures with highlighted components. The first percolation transition is thought to take place at $\chi = 0.25$ and shortly afterwards the whole system predominantly consists of one connected component and isolated nodes (not shown). The largest component continues to evolve as new bonds appear internally. (b) Evolution of the largest connected component in the cell complex. Nodes represent holes in the former network: node size represents the size of the hole, with smallest nodes corresponding to size 3 and the largest to size 6. The second percolation transition is thought to take place at $\chi = 0.7$, wherein the whole cell complex becomes spanned by a component of an extensive size, which severely restricts mobility of the polymer network.

identified by monitoring the fraction of nodes in the largest connected component. As shown in Figure 4f, the gelation occurs later in bond conversion for shorter linkers. This trend is attributed to a large number of self loops that act as ‘defects’ – they increase the bond conversion without contributing to the expansion of the network. A similar conclusion about the effect of cyclization on the gel point was reported by Elliot *et al.*,^{37,38} where the gel point of TeGDMA was observed to be higher than the gel point of BisGDMA (bisphenol A-glycidyl dimethacrylate), with TeGDMA exhibiting three-folded more cyclization than BisGDMA due to the differences in flexibility of the monomers.

Since the gelation starts rather early, around $\chi = 0.2$, most of the network evolution takes place with the giant component being present. Moreover, around $\chi = 0.4$, the whole network predominantly consists of *one* connected component, plus isolated nodes. This behaviour is illustrated with network snapshots in Figure 3a. Surprisingly, the connected network undergoes another structural transition, long after the onset of gelation. We demonstrate this by analysing the *cell complex*^{39–41} which builds upon the idea of a topological hole. Our construction of the cell complex can be thought of as a higher order network in which the nodes are identified with the holes in the original polymer network, and two cell-nodes are connected if the corresponding holes share vertices,⁴² see Figure 3b. This definition allows us to identify connected components in the cell complex and calculate their size. The sizes of the largest component in the cell complex, see Figure 4f, suggest that such a construction *also* undergoes a percolation transition, around $\chi = 0.7$, when a percolating cell component emerges. By $\chi = 0.8 - 0.9$, the giant cell complex expands further and incorporates the majority of the nodes. The structure and development of the cell complex resembles a tree-like construction with a small number of higher order cycles, which can be compared to the early stages of the network formation. There is a large difference between a monomer-node in the original network, and the hole-node in the cell complex, namely the latter has less degrees of freedom, as small holes limit the uniaxial rotation of the constituting monomers. A rapid change in the degrees of freedom that occurs in the physical network at the second transition, see Figure 5, may provide a possible reason behind a sudden nonlinearity in $T_g(\chi)$ observed in Figure 2c for all monomer systems. The location of the second transition is affected by sizes of small topological holes, which, in turn, are influenced by monomer conformation dynamics. This mechanism allows monomers of different type to affect T_g , albeit only at late bond conversions after the onset second transition.

2 Discussion and conclusions

In this work we have re-evaluated the causal link between the non-functional form of the monomer precursor and the phys-

ical properties of the resulting polymer material. To this end, we studied diacrylate monomers with different linker length under the presence/absence of a bulky methyl group and showed that network topology plays a role of an intermediary between monomer type and the emergent physical properties. Monomer’s preference to occupy certain coiled states is central to such a mechanism, as it affects formation of topological holes. We do not entirely confirm the random-coil trend,⁴³ longer linker – less loops. For instance, despite being longer than BDDA, the HDDA monomer has a stronger preference to form loops, as was shown by classical and also confirmed by ab initio metastability simulations.

Although the degree distribution, is only weakly affected by the monomer type, the way the edges are arranged in the network is strongly affected as can be seen from the size distribution of topological holes. These differences affect the number of edges it takes to reach the gelation – the moment when an extensive connected component appears and transforms formerly viscous liquid material into an elastic solid. We observed such a transition in two ways: topologically – by monitoring the largest connected component in the network, and physically – by detecting divergence of the tensile modulus from zero. Even though, longer linkers were shown to slightly accelerate gelation, the tensile modulus was found to be smaller for monomers with longer linkers.

We showed that although T_g is not affected by gelation, there exists a novel higher-order percolation transition that drastically ramps up the T_g at late bond conversions. This percolation transition, marks appearance of an extensive *cell complex* that spans the network and therefore constrains its mobility. In a similar way as gelation marks the onset of elastic behaviour in the polymer, the higher order percolation transition makes the material significantly more brittle, as was shown by the T_g tests. Therefore, at late stages, T_g becomes suddenly sensitive to monomer type – one should be capable to influence glass transition temperature by engineering monomers’ shape, *e.g.* by changing linker length or adding non-reactive groups. A parallel can be made here with another type of higher order structures constraining mobility of physical networks – a *k*-core – that is related to the onset of jamming in granular gels.⁴⁴

Even though, we observe strong differences in the polymerisation kinetics as a function of *time* for different monomers, the topological and physical properties are surprisingly similar when reported as a function of *conversion*. Universal behaviour was seen in almost identical degree distributions, numbers of large cycles, and sizes of components far from the percolation transition. Both T_g and Young’s modulus feature linear dependence on the bond conversion with a universal slope at early to intermediate stages of polymerisation. Therefore, depending on what quantities of interest one aims to predict, coarse-grained and macroscopic models may be well justified, for example, when used in the partial differential equations absorbing MD generated data.^{45,46}

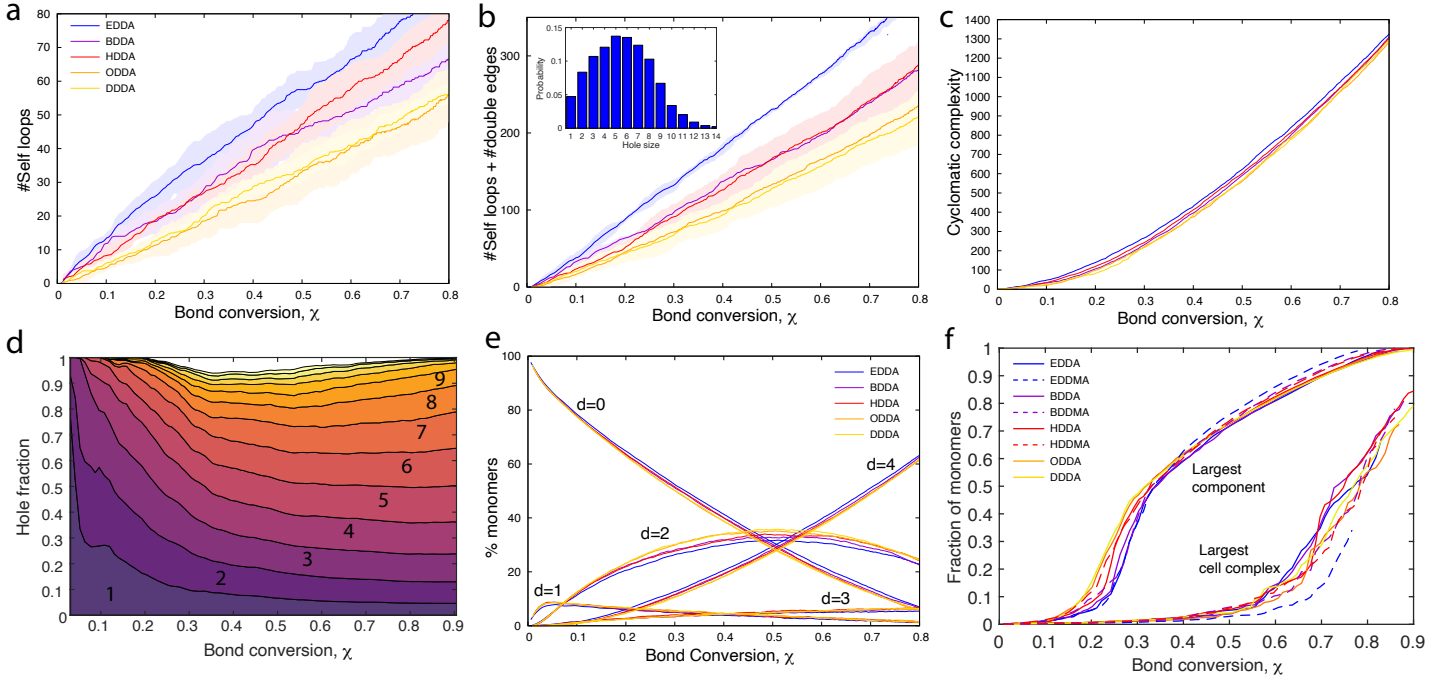


Figure 4: **Graph-theoretical and topological properties of the polymer network.** (a) Number of nodes with one self-loop. (b) Number of nodes with either a double edge or a self loop; the inset shows averaged distribution of hole sizes at $\chi = 0.8$. (c) Universal collapse of the overall cyclomatic complexity. (d) The fraction of holes of indicated size as a function of bond conversion. All networks have 2000 nodes. Supplementary Figure S12 reports hole statistics for each monomer separately. (e) Evolution of the degree distribution. Fractions of nodes with d neighbours show universal dependence for all linker lengths. (f) Universal collapse of the sizes of the largest component and cell complex in different systems. The largest connected components traverses percolation transitions between $\chi = 0.15$ and $\chi = 0.25$ depending on the monomer type. The sizes of the largest connected cell complex feature a second percolation transition around $\chi = 0.7$. Supplementary Figure S11 reports the confidence intervals.

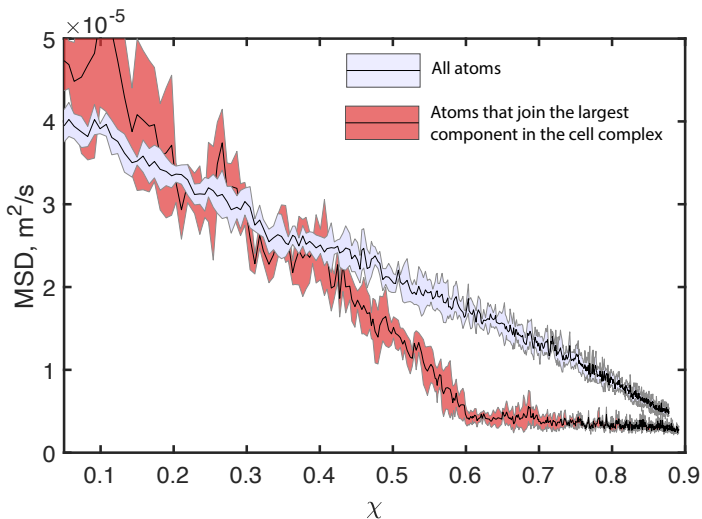


Figure 5: **Mean square displacement (MSD) of atoms in the EDDA system during curing.** The figure demonstrates a separation of the network into two phases with respect to fluctuations. In average the MSD of all atoms decreases with curing, however, the atoms that eventually join the largest connected component in the cell complex (identified at $\chi = 0.6$) reach the terminal MSD earlier than the average atom in the system.

3 Methods

MD model and system set-up

The monomers were modelled at a united-atom (UA) coarse-grained level with the TraPPE-UA force field by Maerzke *et al.*⁴⁷ developed for acrylates. The covalent bonds were represented by a harmonic potential as opposed to rigid bonds, which is necessary for the crosslinking simulations. See Tables 1-4 in the Supportive Information in reference⁷ for the functional form of the force field.

The initial systems were set up by randomly packing 2000 monomers in a 3D simulation cell (initial size $200 \times 200 \text{ \AA}$) with periodic boundary conditions. The systems were then equilibrated in the NVT ensemble at 600 K for 10 ps using a time step of 0.1 fs and further equilibrated in the NPT ensemble at 600 K for 500 ps with a time step of 1 ps. This resulted in a three-dimensional periodic simulation boxes of around $100 \times 100 \text{ \AA}$. The simulations were carried out using the Nosé-Hoover thermostat,^{48,49} and, in the constant pressure cases, using the Martyna-Tuckerman barostat.⁵⁰ From the 2000 monomers units, 5% were considered active at the beginning. This results in a higher radical concentrations than typically used in experiments, however lowering the radical concentrations would make simulations impossibly long. For the effect on the initial amount of radicals on the network formation, see Section 4 and Figures S6 and S7 in.⁷

To validate force field and study the properties of the liq-

uid monomers at ambient conditions, such as density, self-diffusivity and the viscosity of the system, the equilibrated systems at 600 K were cooled down using the NPT ensemble from 600 K to 300 K and further equilibrated for 500 ps at 300 K. The equilibrated systems at 300 K were then used as input for longer simulations at 300 K in the NVT ensemble to determine the density, self-diffusivity and viscosity properties of the melts, which are in a good agreement with experimental values, see Supplementary Table S1. For the viscosity, a correlation time of 1 ns was used and the simulations were run for 500 ns. Further validation of the force field was done by comparing histograms and radial distribution functions (RDFs) of HDDA to *ab-initio* based molecular dynamics (AIMD) simulations as implemented in the CP2K software.⁵¹ AIMD simulations were performed using the BLYP functional supplemented with D3 dispersion corrections.^{17,52} As shown in Supplementary Figure S1 and Supplementary Figure S2, the histogram of the dihedral angles of HDDA in liquid state and the end-to-end distance in HDDA are well captured by the TraPPE-UA force field with a few notable differences. Additionally, the RDFs of the 1-1 and 2-2 reactive sites are also well-captured by the employed force field in comparison to the AIMD simulations as shown in Supplementary Figure S3.

Curing simulations

We used a simulation protocol that accelerates the curing process by lowering activation energies and increasing temperature to 600 K, which was earlier shown not affect the structure of the network when considered as a function of bond conversion.⁷ The covalent bonds appearing during the curing of the network were created using a reactions cutoff radius of 4 Å. The proximity of reactive sites was checked every 10 ps and a bond was created with probability 0.5 for every time reactive sites within the cutoff radius. The activation energy, which affects the chemical reaction rate was assumed to be equal for all monomers. Hence, to link the simulation time to the real time, one needs additionally to compensate the contribution of the chemical activation energy.

The curing of (meth)acrylates involves the addition of radicals to the unsaturated double bonds in the vinyl groups. Assuming the initial reactive radical sites are specified, the curing was implemented in three consecutive steps: (1) the addition of a bond to the unsaturated carbon that undergoes a reaction, (2) the change of the carbon character from unsaturated to saturated (to prevent it from participating in future reactions), and (3) the propagation/regeneration of the reactive site by changing the character of the neighbouring carbon from unsaturated to the reactive one. The curing simulations and the tests for physical properties were repeated four times to average out the effect of fluctuations.

Calculations for T_g

The glass transition temperature was obtained by performing NPT simulations for a series of different temperatures. The systems were cooled down from 600 K to 150 K at the rate of $5 \cdot 10^{-9} \text{ K s}^{-1}$. We determined T_g by analysing the inverse density as a function of temperature²³ and performing a piece-linear fit. In order to identify T_g and quantify the uncertainty that arises due to the finite system size and the thermal fluctuations we introduce the following protocol for statistical inference: First, we solved the minimisation problem

$$j^* = \arg \min_j \sum_{i=1}^j \|r_{i,1}\|_2 + \sum_{i=j+1}^n \|r_{i,2}\|_2$$

where

$$\begin{aligned} r_{i,1} &= \rho_i^{-1} - (\beta_{j,1} T_i + \varepsilon_{j,1}), \\ r_{i,2} &= \rho_i^{-1} - (\beta_{j,2} T_i + \varepsilon_{j,2}), \end{aligned}$$

are the residuals of least square linear fits that correspond to the first $(\rho_i, T_i, i = 1, \dots, j)$ and second $(\rho_i, T_i, i = j + 1, \dots, n)$ fragments of data points separated by index j ; $\rho_i, i = 1, \dots, n$ are the measured density at temperatures T_i , and $\beta_{j,k}, \varepsilon_{j,k}, k = 1, 2$ are the coefficients of the fits. We then define the glass transition temperature as the point where the linear fits intersect:

$$T_g = \frac{\varepsilon_{j,2} - \varepsilon_{j,1}}{\beta_{j,1} - \beta_{j,2}}.$$

Even though ρ_i^{-1} are normally distributed around their fits, T_g is defined as a quotient, and therefore, is not normally nor symmetrically distributed. In fact the distribution for T_g may even contain a heavy tail when the intersection angle is close to π . We thus estimate the confidence intervals for T_g by using a sampling method. Let us denote the averages of the first and second intervals as $\langle x_i \rangle_1 := \frac{1}{j^*} \sum_{i=1}^{j^*} x_i$ and $\langle x_i \rangle_2 := \frac{1}{n-j^*+1} \sum_{i=j^*+1}^n x_i$. We define

$$\sigma_1^2 := \langle T_i \rangle_2^2 \frac{\langle r_{i,1}^2 \rangle_1 - \langle r_{i,1} \rangle_1^2}{\langle T_i^2 \rangle_1 - j^* \langle T_i \rangle_1^2} + \langle T_i \rangle_1^2 \frac{\langle r_{i,1}^2 \rangle_2 - \langle r_{i,1} \rangle_2^2}{\langle T_i^2 \rangle_2 - (n - j^* + 1) \langle T_i \rangle_2^2}$$

and

$$\sigma_2^2 := \frac{\langle r_{i,1}^2 \rangle_1 - \langle r_{i,1} \rangle_1^2}{\langle T_i^2 \rangle_1 - j^* \langle T_i \rangle_1^2} + \frac{\langle r_{i,1}^2 \rangle_2 - \langle r_{i,1} \rangle_2^2}{\langle T_i^2 \rangle_2 - (n - j^* + 1) \langle T_i \rangle_2^2}.$$

Let $X_i \sim \mathcal{N}(\varepsilon_{j,2} - \varepsilon_{j,1}, \sigma_1^2)$ and $X_i \sim \mathcal{N}(\beta_{j,1} - \beta_{j,2}, \sigma_2^2)$ be N independently generated samples generated from the normal distribution $\mathcal{N}(\mu, \sigma^2)$ with mean μ and variance σ^2 . Then $Z_i = \frac{X_i}{Y_i}$ are random samples from the distribution for the T_g estimate. The confidence interval for T_g are the percentiles of the empirical density function for $Z_i - \langle Z_i \rangle$.

Calculation of Young's modulus

To determine Young's modulus, we performed uniaxial tension loading simulations by increasing the length of the simulation cell along the loading direction at every MD step while maintaining atmospheric pressure in the transverse directions using a barostat. Young's modulus was determined by estimating the slope of the stress-strain curve in the linear region, when a sample is pulled at a constant rate in the static tensile test. The stress-strain curves were obtained by applying a uniaxial deformation along the x -axis at a constant rate and measuring the strain-stress response curves. The limit of the longitudinal strain was set to be 50%, and the strain rate was varied between $10^{-7} - 10^{-5} \text{ s}^{-1}$ showing no apparent dependence of inferred Young's modulus on the rate, see Supplementary Figure S16. The strain was determined from $L(t) = L_0 \times \exp(\text{rate} \times dt)$, where $L(t)$ and L_0 are respectively the instantaneous and initial length of the simulation box in the direction of elongation. The stress was calculated from the virial expansion. The transverse directions were maintained at atmospheric pressure using the Martyna-Tuckerman barostat.⁵⁰ Since the test was performed under conditions of thermal fluctuations, as illustrated in Figure 2d, we used Ljung-Box Q-Test to determine if fluctuations around the linear fit for the first $j = 2, 3, \dots$ data-points are pair-correlated. Then, if the identified fragment of the data series passed the Kolmogorov Smirnov test for normality, the slope and its confidence interval were deduced applying the linear regression. This procedure was repeated for different conversions χ and different monomer types, as reported in Supplementary Figure S15. All data points together with their confidence intervals across conversion range were fitted again with a starting line, as shown in Figure 2e. The 'fuzziness' of the latter fits comes from the fact that the data points in the latter fits are supplemented with confidence intervals, and therefore, such secondary fits are drawn from a probability distribution.

Average resistance model for elasticity

The approximation of the elastic modulus was obtained using the graph resistance model:

$$E^* = C \left(\frac{1}{|\Omega_1| |\Omega_2|} \sum_{i \in \Omega_1, j \in \Omega_2} (L_{i,i}^+ + L_{j,j}^+ - L_{i,j}^+ - L_{j,i}^+) \right)^{-1},$$

where C is a constant that represents monomer tendency to coil and (was estimated from molecular simulations), $\mathbf{L} = \mathbf{D} - \mathbf{A}$ is the graph laplacian with \mathbf{D} being the diagonal matrix with node degrees on the diagonal and \mathbf{A} the adjacency matrix of the monomer network and \mathbf{L}^+ indicating its Moore-Penrose inverse; Ω_1 and Ω_2 are the index sets for monomers that are located at the two opposite faces of the simulation box. This estimate is based on the electrical engineering concept of effective resistance.⁵³

Acknowledgements

ATK and VS acknowledge the financial support from the Netherlands Organisation for Scientific Research (NWO) via respectively project PREDAGIO and Open Technology Program.

Author contributions

ATK and VS – high-performance computing and molecular dynamics, NG – *ab initio* simulations, PDI – chemical context, IK – research design and network topology analysis. All authors discussed results and contributed to writing.

Additional information

The authors report no competing interests.

References

- [1] Cinar, S. A.; De Proft, F.; Avci, D.; Aviyente, V.; De Vleeschouwer, F. *Macromolecular Chemistry and Physics* **2015**, *216*, 334–343.
- [2] Jung, J.; Park, C.; Yun, G. J. *European Polymer Journal* **2019**, *114*, 223–233.
- [3] Demir, B.; Walsh, T. R. *ACS Applied Polymer Materials* **2019**,
- [4] Huang, M.; Abrams, C. *Macromolecular Theory and Simulations* **2019**, 1900030.
- [5] Klähn, M.; Krishnan, R.; Phang, J. M.; Lim, F. C.; van Herk, A. M.; Jana, S. *Polymer* **2019**, *179*, 121635.
- [6] Rudyak, V.; Efimova, E.; Guseva, D.; Chertovich, A. *Polymers* **2019**, *11*, 36.
- [7] Torres-Knoop, A.; Kryven, I.; Schamboeck, V.; Iedema, P. D. *Soft Matter* **2018**, *14*, 3404–3414.
- [8] others., et al. *Proceedings of the National Academy of Sciences* **2020**, *117*, 11299–11305.
- [9] Lu, H.; Stansbury, J. W.; Nie, J.; Berchtold, K. A.; Bowman, C. N. *Biomaterials* **2005**, *26*, 1329–1336.
- [10] Tran, K. T.; Nguyen, T. D. *Journal of Science: Advanced Materials and Devices* **2017**, *2*, 1–14.
- [11] Moszner, N.; Salz, U. *Prog. Polym. Sci.* **2001**, *26*, 535–576.
- [12] Decker, C.; Viet, T. N. T.; Decker, D. *Polymer* **2001**, *42*, 5531–5541.
- [13] Yao, B.; Zhao, H.; Wang, L.; Liu, Y.; Zheng, C.; Li, H. *J. Coat. Technol. Res.* **2018**, *15*, 149–158.
- [14] Anseth, K. S.; Burdick, J. A. *MRS Bull.* **2002**, *27*, 130–136.
- [15] Fisher, J. P.; Dean, D.; Engle, P. S.; Mikos, A. G. *Annu. Rev. Mater. Res.* **2001**, *31*, 171–181.
- [16] Van Steenberge, P. H.; Sedlacek, O.; Hernández-Ortiz, J. C.; Verbraeken, B.; Reyniers, M.-F.; Hoogenboom, R.; D’hooge, D. R. *Nature communications* **2019**, *10*, 1–14.
- [17] Gao, Y.; Zhou, D.; Lyu, J.; Sigen, A.; Xu, Q.; Newland, B.; Matyjaszewski, K.; Tai, H.; Wang, W. *Nature Reviews Chemistry* **2020**, 1–19.
- [18] Kryven, I. *Phys. Rev. E* **2016**, *94*, 012315.
- [19] Kryven, I. *Phys. Rev. E* **2017**, *95*, 052303.
- [20] Kryven, I. *Journal of Mathematical Chemistry* **2018**, *56*, 140–157.
- [21] Schamboeck, V.; Iedema, P. D.; Kryven, I. *Scientific reports* **2019**, *9*, 1–18.
- [22] Kurdikar, D. L.; Peppas, N. A. *Polymer* **1994**, *35*, 1004–1011.
- [23] Yang, Q.; Chen, X.; He, Z.; Lan, F.; Liu, H. *Rsc Advances* **2016**, *6*, 12053–12060.
- [24] Kannurpatti, A. R.; Anseth, J. W.; Bowman, C. N. *Polymer* **1998**, *39*, 2507–2513.
- [25] Jerolimov, V.; Jagger, R. G.; Millward, P. J. *Atca Stomatol. Crota.* **1994**, *28*, 3–9.
- [26] Cook, W. D.; Moopnar, M. *Biomaterials* **1990**, *11*, 272–276.
- [27] Davis, T. P.; Huglin, M. B.; Yip, D. C. *Polymer* **1988**, *29*, 701–706.
- [28] Luo, K.; Wangari, C.; Subhash, G.; Spearot, D. E. *The Journal of Physical Chemistry B* **2020**, *124*, 2029–2039.
- [29] Sirk, T. W. *Proceedings of the National Academy of Sciences* **2020**,
- [30] Gu, Y.; Kawamoto, K.; Zhong, M.; Chen, M.; Hore, M. J. A.; Jordan, A. M.; Korley, L. T. J.; Olsen, B. D.; Johnson, J. A. *Proceedings of the National Academy of Sciences* **2017**, *114*, 4875–4880.
- [31] Zhong, M.; Wang, R.; Kawamoto, K.; Olsen, B. D.; Johnson, J. A. *Science* **2016**, *353*, 1264–1268.
- [32] Wang, R.; Alexander-Katz, A.; Johnson, J. A.; Olsen, B. D. *Phys. Rev. Lett.* **2016**, *116*, 188302.

- [33] Stanley, H. E.; Blumberg, R. L.; Geiger, A. *Physical Review B* **1983**, *28*, 1626.
- [34] Schamboeck, V.; Iedema, P. D.; Kryven, I. *Scientific Reports* **2020**, *10*, 1–18.
- [35] Schamboeck, V.; Kryven, I.; Iedema, P. D. *Physical Review E* **2020**, *101*, 012303.
- [36] Kryven, I. *Nature communications* **2019**, *10*, 1–16.
- [37] Elliott, J. E.; Lovell, L. G.; Bowman, C. N. *Dent Mater.* **2001**, *17*, 221–9.
- [38] Elliott, J. E.; Bowman, C. N. *Macromolecules* **1999**, *32*, 8621–8628.
- [39] Battiston, F.; Cencetti, G.; Iacopini, I.; Latora, V.; Lucas, M.; Patania, A.; Young, J.-G.; Petri, G. *arXiv preprint arXiv:2006.01764* **2020**,
- [40] Bianconi, G.; Kryven, I.; Ziff, R. M. *Physical Review E* **2019**, *100*, 062311.
- [41] Kryven, I.; Ziff, R. M.; Bianconi, G. *Physical Review E* **2019**, *100*, 022306.
- [42] Iacopini, I.; Petri, G.; Barrat, A.; Latora, V. *Nature communications* **2019**, *10*, 1–9.
- [43] Flory, P. J. *Polymer* **1979**, *20*, 1317–1320.
- [44] Morone, F.; Burleson-Lesser, K.; Vinutha, H.; Sastry, S.; Makse, H. A. *Physica A: Statistical Mechanics and its Applications* **2019**, *516*, 172–177.
- [45] Park, C.; Jung, J.; Yun, G. J. *International Journal of Plasticity* **2020**, 102680.
- [46] Alamé, G.; Brassart, L. *Soft matter* **2019**, *15*, 5703–5713.
- [47] Maerzke, K. A.; Schultz, N. E.; Ross, R. B.; Siepmann, J. I. *J. Phys. Chem. B* **2009**, *113*, 6415–6425.
- [48] Hoover, W.; Ladd, A. J. C.; Moran, B. *Phys Rev Lett.* **1982**, *48*, 1818–1820.
- [49] Nosé, S. *J. Chem. Phys.* **1984**, *81*, 511–519.
- [50] Tuckerman, A.; Lopez-Rendon, J.; Martyna, A. *J Phys A: Math Gen* **2006**, *39*, 5629.
- [51] Kühne, T. D. et al. *The Journal of Chemical Physics* **2020**, *152*, 194103.
- [52] Grimme, S.; Antony, J.; Ehrlich, S.; Krieg, H. *The Journal of Chemical Physics* **2010**, *132*, 154104.
- [53] Ellens, W.; Spieksma, F.; Van Mieghem, P.; Jankovic, A.; Kooij, R. *Linear algebra and its applications* **2011**, *435*, 2491–2506.